Hindawi
Journal of Advanced Transportation
Volume 2019, Article ID 9127062, 19 pages
https://doi.org/10.1155/2019/9127062

Research Article

Modeling and Simulation of Nonmotorized Vehicles' Dispersion at Mixed Flow Intersections

Qiyuan Liu, Jian Sun, Ye Tian, Ying Ni, and Shinan Yu

Key Laboratory of Road and Traffic Engineering in the Ministry of Education, Tongji University, Shanghai 201804, China

Correspondence should be addressed to Ye Tian; tianye@tongji.edu.cn

Received 15 October 2018; Revised 31 December 2018; Accepted 13 January 2019; Published 5 March 2019

Academic Editor: Juan C. Cano

Copyright © 2019 Qiyuan Liu et al. This is an open access article distributed under the Creative Commons Attribution License, which permits unrestricted use, distribution, and reproduction in any medium, provided the original work is properly cited.

Interactions between motorized and nonmotorized vehicles have drawn considerable attention from researchers. They are commonly seen at mixed flow intersections where nonmotorized vehicles, without the restriction of lane markers or physical barriers, may disperse into adjacent lanes and thus lead to complex interactions with motorized vehicles. Such a dispersion phenomenon between heterogeneous participants (e-bikes and bicycles as nonmotorized vehicles versus motorized vehicles) is difficult to model. In this paper, we were inspired by the dispersion of charged particles in an electric field and modeled the dispersion phenomenon of go-straight, nonmotorized vehicles at mixed flow intersections accordingly, as it was discovered in this research that these two dispersion phenomena share three underlying commonalities with each other. A novel particle dispersion model (PDM) based on a particle's movement in an electric field is proposed. The model is calibrated and validated using 1,490 high-definition sets of trajectory data for go-straight, nonmotorized vehicles during 43 cycles at two typical mixed flow intersections. The PDM is compared with the social force model (SFM) on their dispersion characteristics that are used to describe the nonmotorized bicycles' behavior. The results show that the PDM performs better than the SFM with regard to depicting the dispersion characteristic indices of the nonmotorized vehicles, such as the travel time, the dispersion intensity of heterogeneous nonmotorized vehicles, the sectional dispersion degree, and other dispersion characteristics.

1. Introduction

Nonmotorized vehicles have a great impact on the safety and efficiency of mixed flow intersections. Accurately depicting the interactions between motorized and nonmotorized vehicles has important ramifications regarding improving safety [1–3] and evaluating the capacity [4, 5] of intersections. Previous studies paid more attention to the interactions between motorized and nonmotorized vehicles that have temporal or spatial crossing conflicts, such as the conflict between left-turn, nonmotorized vehicles and opposing go-straight motorized vehicles [6] and between go-straight, nonmotorized vehicles and left-turn/right-turn motorized vehicles [7–10]. Recent studies have shown that the safety and efficiency of these intersections can decline as well due to interactions without any crossing conflict [11, 12]. One of the most common interactions is the lateral interaction between nonmotorized and motorized vehicles driving in the same direction (e.g., go-straight, left-turn) because of the dispersion phenomenon of nonmotorized vehicles. The term dispersion phenomenon [13] refers to a situation where after nonmotorized vehicles move across a mixed flow intersection, some of them will disperse laterally into the adjacent motorized vehicle lane or crosswalk without being restricted by a lane marker or physical barrier. This phenomenon can result in nonmotorized vehicles' laterally dispersing outside their presumed driving space (the yellow dashed line drawn based on the lane markers of the sequential roadway segment in Figure 1(a)) and thus invading the motorized vehicles' driving space. During the whole crossing process in each cycle, the group of nonmotorized vehicles will disperse at the beginning and shrink near the end (Figure 1(c)), resulting in an elliptical driving space (Figure 1(b)).

Modeling the dispersion phenomenon of nonmotorized vehicles is therefore of great significance. First, it helps predict the driving zone of the nonmotorized vehicles and thus can indicate potential guidelines with regard to the design of lane markers or the intersections themselves in order to further

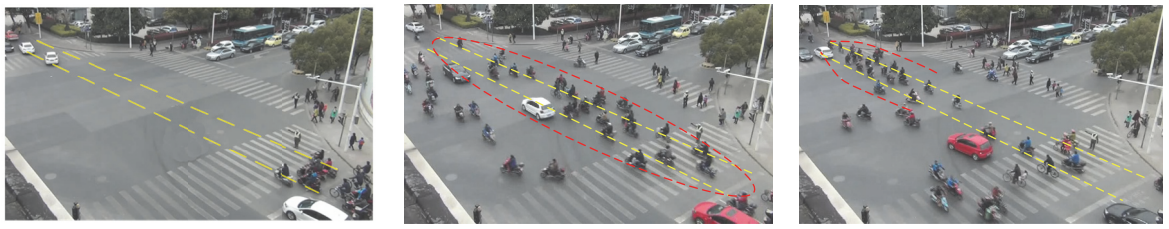

(a) t=0s (b) t=5s (c) t=10s

Figure 1: Dispersion phenomenon at a mixed flow intersection.

the safety of mixed flow intersections [14]. Second, it is useful to estimate the saturation flow of motorized vehicles when the nonmotorized vehicle group disperses [15] into the motorized vehicles' lane. Third, it helps to develop a heterogeneous traffic simulation model with high accuracy. Lastly, it helps driverless vehicles foresee abnormal behavior of nonmotorized vehicles at intersections.

To date, there is a lack of knowledge and understanding as to what the principle factors that influence how nonmotorized vehicles disperse are and what the best approach to model such dispersion is. There are two main challenges to this problem. First, the diversity of interaction objects is complex (including dispersing nonmotorized and motorized vehicles) and the nonmotorized vehicles are heterogeneous (including e-bikes and bicycles) [16]. The inherent stochastic nature is thus introduced because of the heterogeneity of the traffic flow. Second, the abnormal trajectories of dispersion, which resemble serpentine routes in unlimited driving space, are difficult to predict and model at mixed flow intersections.

To overcome these challenges and model the dispersion phenomenon, 1,490 high-definition trajectories of nonmotorized vehicles were collected for 43 cycles in total at two intersections in Shanghai. Meanwhile, the motorized vehicle trajectory data was collected for the adjacent lane. The following contributions are made in this study. (1) Using field data, the dispersion characteristics of the heterogeneous nonmotorized vehicle flow was analyzed. The different characteristics between the e-bikes and the bicycles were compared. (2) A novel particle dispersion model (PDM) was proposed to model the dispersion behavior of nonmotorized vehicles. This model is derived from charged particles' dispersion in an electric field. (3) A simulation prototype was established using this PDM and the results generated by the PDM were compared with that of a classic social force model (SFM). The results show that the PDM performs better than the SFM, as it is capable of simulating the dispersion of the nonmotorized vehicle flow and has a higher accuracy when describing dispersion characteristics.

2. Literature Review

Two groups of literature are related to the dispersion phenomenon of nonmotorized vehicles: (1) research on the moving characteristics of nonmotorized vehicles, and (2) the interaction models between motorized and nonmotorized vehicles in general. Literature in those two groups is reviewed in this section.

In their study on a group of nonmotorized vehicles, Khan and Maini [17] reviewed the maneuverability and interaction characteristics of nonmotorized vehicles under non-lane-based traffic from many researchers, but the dispersion maneuver had yet to be put forth. Lin and Wu [18] observed and surveyed the mean crossing speed and the acceptance critical gap in between nonmotorized vehicles. Wang et al. [16] analyzed the conversion factor of go-straight, nonmotorized vehicles based on the relationship between the flow rate of nonmotorized vehicles and the flow rate of motorized vehicles for different crossing times. Similarly, dispersion was not yet considered in this research. To date, only two projects were found to emphasize the dispersion characteristics of go-straight, nonmotorized vehicles. Jiang et al. [19] surveyed the clearance time of the dispersion of nonmotorized vehicle groups and compared it with a situation without dispersion.

There are many models used to depict nonmotorized vehicles. A summary of existing models can be found in Twaddle et al. [20]. These models can be divided into three groups: the virtual lane models in simulation tools, the social force models (SFM), and the cellular automation (CA) models. Barceló [21] introduced the virtual lane model for nonmotorized vehicles in practice simulation tools such as VISSIM, Aimsun, and SUMO. In these simulation tools, the dispersion phenomenon cannot be expressed because the models are one-dimensional. The SFM was first proposed by Helbing and Molnar [20] to model pedestrians and was later widely adapted to depict nonmotorized vehicles' behavior [22, 23]. There are three forces considered in the SFM during the process when nonmotorized vehicles move to a destination: the driving force to the destination, the repulsive force from other nonmotorized vehicles, and the boundary force. Some researchers further developed the SFM to model nonmotorized vehicles sophistically. Liang et al. [24] developed a SFM in which if two nonmotorized vehicles came close enough, a physical model took over to prevent a collision. Schönauer et al. [25] used a three-level model to depict the behavior of mixed flow traffic: an infrastructure model, an operational model, and a tactical model. All the prior studies using the SFM have not referred to the dispersion phenomenon of nonmotorized vehicles. The disadvantages of SFM when depicting the dispersion phenomenon are that the dispersion direction of a nonmotorized vehicle is usually flexible during the process of dispersion and shrinkage, while the direction is

fixed in the SFM. The CA model is a time and space discrete model and it was proposed by Nagel and Schreckenberg [26]. In the CA model, the road segment is divided into cells, and the model was used to emulate motorized vehicles at first. Vehicles use four regimes to move in the grid of cells: acceleration, deceleration, randomization, and update. Yao et al. [27] divided the shared space into a 1 m∗1m grid to simulate the interaction between nonmotorized vehicles and motorized vehicles. These interactions are classified into two types: friction and blockage. Luo et al. [28] divided the nonmotorized vehicle lane more precisely, and the lateral movement rules and front movement rules were given for nonmotorized vehicles. Ren et al. [13] divided the driving zone into a 1 m∗1m grid where the nonmotorized vehicles would disperse into the lateral margin grid if the volume of the nonmotorized vehicles exceeded a certain threshold. The authors compared the clearance time with different e-bike ratios. However, the microdispersion characteristics, such as the dispersion ratio or the dispersion degree of nonmotorized vehicles, were not analyzed. Along this line of research, Jiang et al. [19] set up a similar dispersion zone and further established the interaction rules between go-straight, nonmotorized vehicles and go-straight motorized vehicles. Two major shortcomings exist for CA models when applied to depicting dispersion phenomenon. First, the difference in the dispersion characteristics of the heterogeneous e-bikes and bicycles cannot be described. Second, the dispersion boundary of the cells is fixed in CA models, while boundaries in reality are observed to be varying from cycle to cycle.

In summary, there are studies on the characteristics of nonmotorized vehicles while very few of them focused on the dispersion phenomenon. The existing studies on dispersion phenomena are mostly empirical analysis with only the macroindex considered. The microscopic behavioral mechanism of the heterogeneous e-bikes and bicycles is never considered. Therefore, existing models cannot be adopted to accurately simulate the dispersion phenomenon, meaning a new model is necessary. This paper puts forward a novel PDM to overcome these challenges, and the improvements and innovation of the model compared to existing ones are as follows.

(a) The most important characteristic of the dispersing go-straight, nonmotorized vehicles is that their moving direction is dynamic during the crossing process. The existing model including the well-received SFM and CA model could only generate a fixed direction for nonmotorized vehicles and thus would omit such influential dispersing characteristics. The proposed PDM could capture such pattern with dispersing nonmotorized vehicles heading towards outside of their lane to find a comfort space to move with a high speed, while heading back to inside of the lane to exit the intersection.

(b) The different nonmotorized vehicles with different desired speeds (such as bicycles and e-bikes) would have different dispersion intensity. The PDM can capture such a phenomenon.

(c) The PDM has fewer parameters that need to be calibrated compared to the SFM and CA model.

3. Data Collection and Preliminary Analysis

3.1. Data Collection. To model the dispersion phenomenon of nonmotorized vehicles at mixed flow intersections, the high-definition trajectory data of dispersing nonmotorized vehicles was utilized. Specifically, the trajectories were collected for go-straight, nonmotorized vehicles from the east bound entrance of two mixed flow intersections in Shanghai during evening peak hours (16:30-17:30 as per the observations at the intersections). One is the Changji-Moyu intersection, and the other is the Xianxia-Jianhe intersection. The geometric designs of the two intersections are similar, as there is no lane marker at the intersections (shown in Figure 2) and go-straight, nonmotorized vehicles are composed of both e-bikes and bicycles. A video trajectory processing software [29, 30] was utilized to extract the time-space trajectory data of the go-straight, nonmotorized vehicles and the motorized vehicles in the adjacent lane (Figure 2) at the intersections. The trajectory data frequency is 0.12s, and the positional accuracy is 0.05m. Such high-definition data is adequate to ensure the reliability of the analysis results. A total of 830 go-straight, nonmotorized vehicles' trajectory data during 19 cycles at the Changji-Moyu intersection and 660 go-straight nonmotorized vehicles' trajectory data during 24 cycles at the Xianxia-Jianhe intersection were collected. The channelization design of the two intersections and a screenshot of the video processing software are shown in Figure 2.

The cycle lengths are 152 seconds (s) at the Changji-Moyu intersection and 138s at the Xianxia-Jianhe intersection. In this study, it was decided to analyze the dispersion characteristics at the most typical intersection, so those two typical major arterial intersections were selected. The width of the nonmotorized vehicle lane is 3.5 meter (m). 3.5m is one of the commonly suggested nonmotorized vehicle lane width listed in the national standard of Chinese transport planning on urban road [31]. Such configuration has been utilized in most recent research articles on nonmotorized vehicles' behavior in China [13, 32, 33]. The lengths of the intersections are 47 m at the Changji-Moyu intersection and 50 m at the Xianxia-Jianhe intersection. The average speed of the e-bikes and bicycles is 6.59 m/s and 4.44 m/s, respectively, at the Changji-Moyu intersection. The average speed of the e-bikes and bicycles is 6.79 m/s and 4.25 m/s, respectively, at the Xianxia-Jianhe intersection. The overall ratio of e-bikes is 70.84% at the Changji-Moyu intersection and 68.33% at the Xianxia-Jianhe intersection.

3.2. Dispersion Characteristics and Influence Factors. Let $d_{i,t}$ denote the lateral offset distance from the lane center to the nonmotorized vehicle i at time t (see Figure 3). The maximum lateral offset distance D_i^{max} can be derived as $D_i^{max} = \max(d_{i,t}), \forall i \in V$, where V denotes the set of nonmotorized vehicles. D_i^{max} (shown in Figure 3) could then be adopted to describe the dispersion intensity of each nonmotorized vehicle. The larger the D_i^{max} is, the more severe the dispersion of nonmotorized vehicle i is. Since the width of the nonmotorized vehicle lane w is 3.5m for both intersections of interest, a D_i^{max} lower than 1.75m denotes a nondispersing nonmotorized vehicle i with low

Figure 2: Channelization design of the two intersections and a screenshot of the trajectory extraction software.

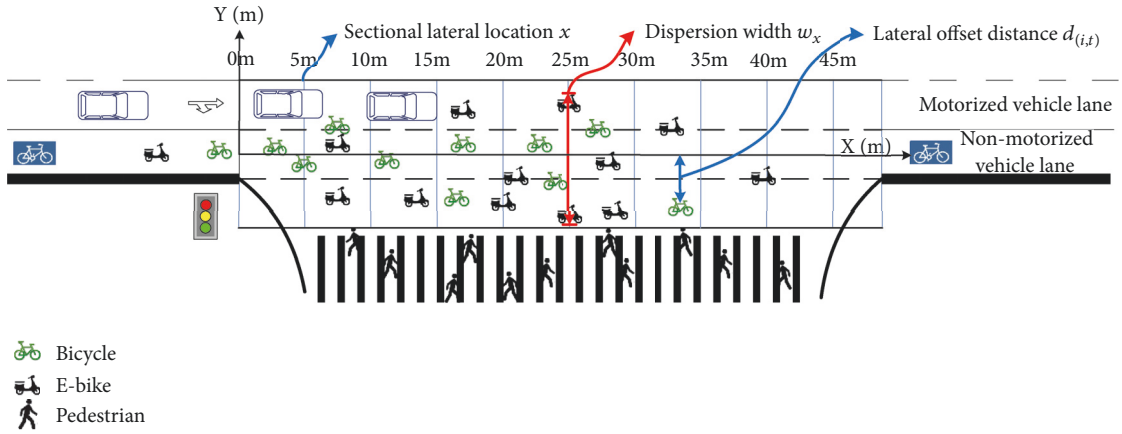

Figure 3: Illustration of the sectional lateral location, the dispersion width and the lateral offset distance.

dispersion intensity. Otherwise, it indicates a dispersing nonmotorized vehicle ($D_i^{max} > 1.75$m) and represents either a nonmotorized vehicle with medium dispersion intensity if $1.75m < D_i^{max} \leq 3.25$m or a nonmotorized vehicle with high dispersion intensity if $D_i^{max} > 3.25$m. 3.25m is selected as the boundary between the two bins because the nonmotorized vehicles start to block motorized vehicles on the left side or influence pedestrians on the right side if $D_i^{max} > 3.25$m based on field data (further discussed in Section 3.4).

The varying dispersion characteristics in each cycle are also of interest, as they reflect the real driving space of the nonmotorized vehicle group at mixed flow intersections. In order to analyze nonmotorized vehicles' dispersion characteristics at each crossing stage in each cycle, a variable called the sectional dispersion degree λ_x is put forward. It is calculated by

$$\lambda_x = \frac{w_x}{w} \tag{1}$$

where x denotes the sectional lateral location of nonmotorized vehicle i. In our study, the intersection is longitudinally divided into 10 sections every 5 meters from 0 m to 50 m, with $x \in [0m, 5m, 10m \ldots, 45m]$. w_x is the dispersion width (shown in Figure 3) at location x. w is the width of the nonmotorized vehicle lane.

3.3. The Critical Dispersion Boundary. The critical boundaries (δ_l^{max} and δ_r^{max}) of the maximum lateral offset distance between the medium and high dispersion intensity can be

obtained from either side of the moving direction and they are not necessarily identical to each other. On the left side, the dispersing nonmotorized vehicles may block motorized vehicles. The *"block" interference (or behavior) is generated when the bicycle occupies part of the motorized vehicle lane and it blocks the way of a motorized vehicle moving forward. In this case, the motorized vehicle has to move at a slower speed, and this is likely to lead to traffic congestion.* This definition was put forward by Zang et al. in 2000 [34] and has been referred to by other researchers afterwards [22, 28, 35, 36]. However, most of the time, there is no lane marker in between the motorized and nonmotorized vehicle lanes at intersections and the motorized vehicles are likely to move inside of the intersection to avoid collisions with nonmotorized vehicles. As such, it is desired to find the critical maximum lateral offset distance δ_l^{max} above which the nonmotorized vehicles start to impact the speed of the rear motorized vehicle.

To obtain δ_l^{max}, the speed of the rear motorized vehicle v_i^{rear} of the dispersing nonmotorized vehicle i (with $D_i^{max} > 1.75$m) inside of the intersection (left side of the nonmotorized vehicles) at the time when the lateral offset distance is D_i^{max} is extracted. $f(D_i^{max})$ denotes the mapping function between D_i^{max} and v_i^{rear}.

$$f\left(D_i^{max}\right) = v_i^{rear} \tag{2}$$

Let i_1 denote the index of a nonmotorized vehicle with D_i^{max} that $1.75m < D_i^{max} \le \delta_l^{max}$. i_2 denotes the index of a nonmotorized vehicle with D_i^{max} that $\delta_l^{max} < D_i^{max}$. Let N_1 and N_2 denote the total number of nonmotorized vehicles i_1 and i_2, respectively. Then, δ_l^{max} could be given by

$$\delta_l^{max} = \operatorname{argmax}\left(\frac{1}{N_1}\sum_{i_1=1}^{N_1} f\left(D_{i_1}^{max}\right) - \frac{1}{N_2}\sum_{i_2=1}^{N_2} f\left(D_{i_2}^{max}\right) \mid D_{i_1}^{max} \le \delta_l^{max} \text{ and } D_{i_2}^{max} > \delta_l^{max}\right) \tag{3}$$

Based on (3), δ_l^{max} is 3.22m at the Changji-Moyu intersection and 3.27m at the Xianxia-Jianhe intersection. The relationships between D_i^{max} and v_i^{rear} for both intersections are shown in Figures 4 and 5.

With such a δ_l^{max}, the average speeds of rear motorized vehicles when $D_i^{max} > \delta_l^{max}$ are 25% and 27.4% lower than that when $D_i^{max} \le \delta_l^{max}$ at two intersections, respectively. Such a speed drop would have a significant influence on the saturation flow of motorized vehicles and is likely to lead to traffic congestion ($v_i^{rear} < 10$km/h) as has been shown in Figures 4 and 5.

The values of δ_l^{max} are close to each other at both intersections. Therefore, 3.25m is selected as the uniform critical value to present the boundary between nonmotorized vehicles with high and medium dispersion intensity for both intersections for the sake of calculation simplicity.

To obtain δ_r^{max} for the right side, the most intuitive approach is to conduct a similar statistical analysis on the speed drop of pedestrians. However, as has been observed in field data, the speed drop of pedestrians due to the blockage of nonmotorized vehicles is not noticeable as compared to the drop for motorized vehicles on the left side since the speeds of pedestrians are generally lower than that of nonmotorized vehicles. In the meantime, the motion of pedestrians because of the impact of nonmotorized vehicles often involves lateral movement. Therefore, the safety distance (>1m) [37, 38] is taken into count to obtain δ_r^{max} for the right side. Figures 6 and 7 present the histograms of safe and unsafe occurrences with respect to the D_i^{max} of nonmotorized vehicles.

The binary logistic model [39] is adopted to find the optimal value of δ_r^{max}. In the binary logistic model, D_i^{max} is set

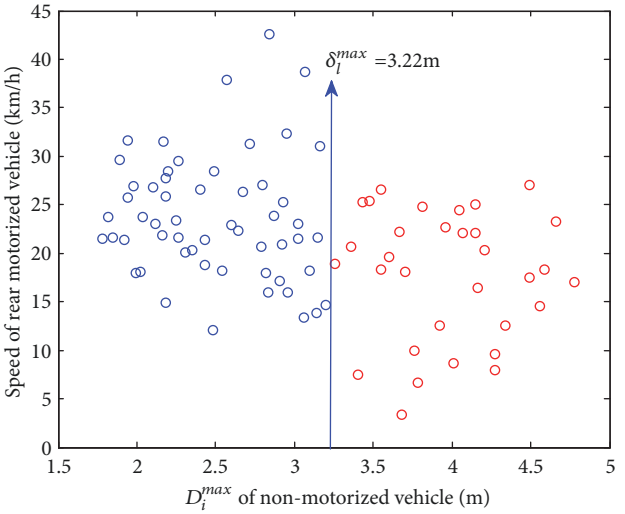

FIGURE 4: Relationship between $\boldsymbol{D_i^{max}}$ and $\boldsymbol{v_i^{rear}}$ at the Changji-Moyu intersection. When $\boldsymbol{\delta_l^{max} = 3.22m}$, the difference between the average speed of rear vehicles when $\boldsymbol{D_i^{max} \ge 3.22\ m}$ and $\boldsymbol{D_i^{max} < 3.22\ m}$ reaches the maximum.

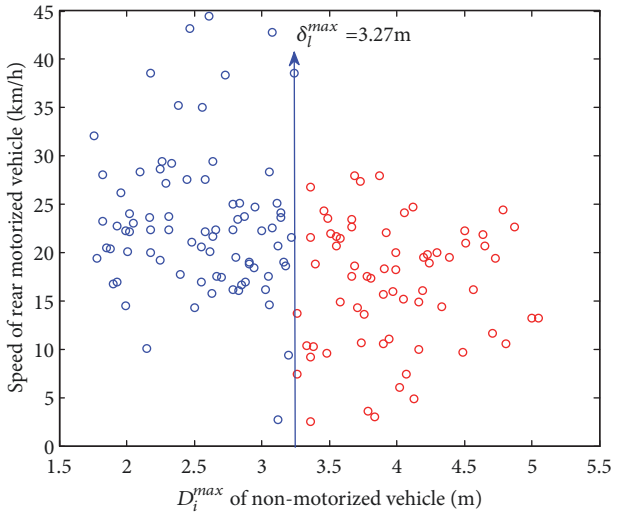

FIGURE 5: Relationship between D_i^{max} and v_i^{rear} at the Xianxia-Jianhe intersection. When $\delta_l^{max} = 3.27m$, the difference between the average speed of rear vehicles when $D_i^{max} \ge 3.27m$ and $D_i^{max} < 3.27m$ reaches the maximum.

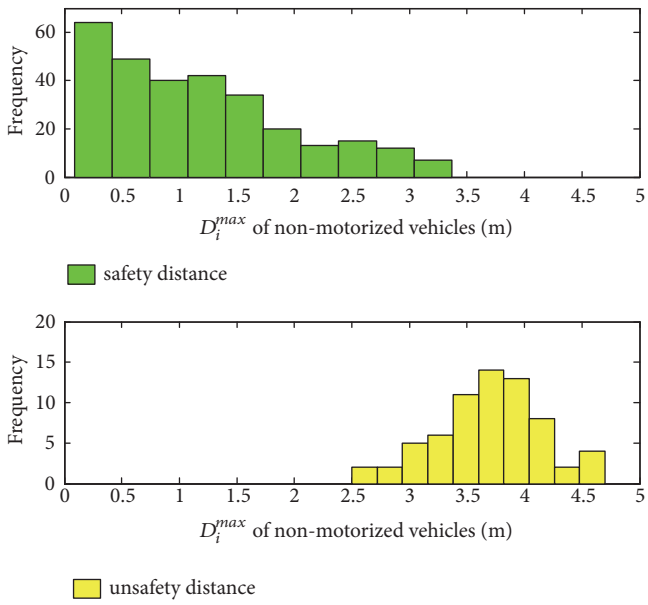

FIGURE 6: Histograms of the safe and unsafe occurrences with respect to the $\boldsymbol{D_i^{max}}$ of nonmotorized vehicles at the Changji-Moyu intersection.

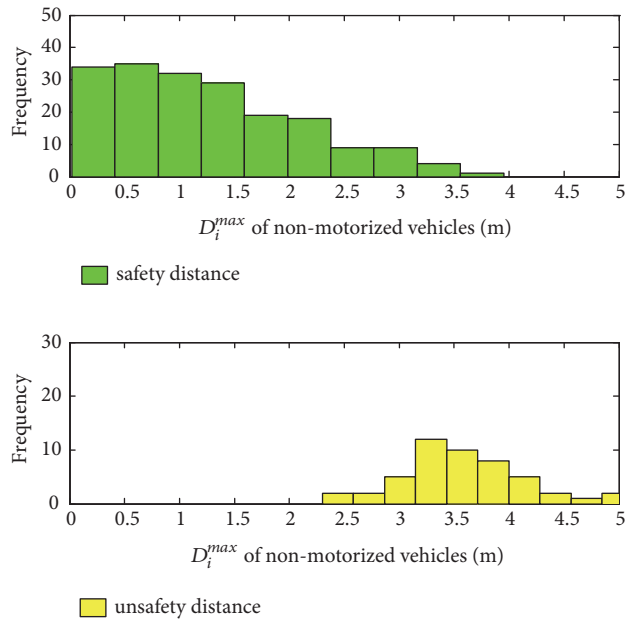

FIGURE 7: Histograms of the safe and unsafe occurrences with respect to the D_i^{max} of nonmotorized vehicles at the Xianxia-Jianhe intersection.

as the independent variable, and whether the nonmotorized vehicle keeps a safe distance to pedestrians is set as the dependent variable. As such, the model has a binary choice result. Let B_1 denote the coefficient of the independent variable D_i^{max} and B_2 as a constant. The formulation of the binary logistic model is given in

$$P\left(D_i^{max}\right) = 1 - \frac{1}{1 + e^{B_1 D_i^{max} + B_2}} \quad (4)$$

When $P(D_i^{max})$ equals 0.5, the value of D_i^{max} can be adopted as δ_r^{max}. The parameters of (4) at two intersections are shown in Table 1.

The results show that the critical boundary of safe and unsafe distances on the right side δ_r^{max} is 3.067m and 3.191m, respectively, at the two intersections. However, 3.25m is again chosen as the boundary between the high dispersion intensity and medium dispersion intensity for the right side for the following reasons.

(a) The operation of motorized vehicles has a greater influence on overall safety and efficiency of the intersection compared to pedestrians. Therefore, the left side boundary is chosen in the study.

(b) The relative discrepancy between 3.067m (or 3.191m) for δ_r^{max} on the right side and 3.25m for δ_l^{max} is less than 6%. For the sake of modeling simplicity, such a difference is omitted and 3.25m is adopted uniformly.

3.4. Dispersion Characteristic Analysis. The maximum lateral offset distance D_i^{max} for all 1,490 go-straight e-bikes and bicycles at both intersections was recorded. The histograms of D_i^{max} (bins for low/medium/high dispersion intensity are marked by green/yellow/red, respectively) are shown in Figure 8 for e-bikes and bicycles, respectively.

From Figure 8 one can tell that the e-bikes have a relatively stronger dispersion intensity compared to bicycles, as the percentage of dispersing e-bikes (including vehicles with medium/high dispersion intensity) is 7.82% higher than that of bicycles at the Changji-Moyu intersection and 12.67% higher at the Xianxia-Jianhe intersection. Moreover, the percentage of high dispersion intensity e-bikes is almost twice of that of bicycles at both intersections. The maximum lateral offset distance D_{max} of e-bikes is also higher than that of bicycles. Therefore, the heterogeneity is observed that the e-bikes are more likely to disperse and have a relatively higher dispersion intensity as compared to bicycles. One may notice that the dispersion intensity at the Xianxia-Jianhe intersection is generally higher than that at the Changji-Moyu intersection, most likely due to the fact that the adjacent motorized vehicle lane at the Xianxia-Jianhe intersection has relatively less volume and thus nonmotorized vehicles are more likely to disperse into the motorized vehicle lane.

The boxplots of the sectional dispersion degree value λ_x are shown in Figures 9 and 10. From these figures one can tell that, in general, the median value of the sectional dispersion degree λ_x increases first and then decreases, which is in agreement with the "dispersion and shrinkage" phenomenon that has been observed in previous literature. However, the geometric pattern of such a "dispersion and shrinkage" phenomenon differs in two intersections. One can tell that the dispersion zone of the Changji-Moyu intersection tends to be longer than that of the Xianxia-Jianhe intersection. In the meantime, the dispersion intensity is higher at the Changji-Moyu intersection as the dispersion degree raises up to a high level and then stays flat for roughly 35 meters and then decreases within the last two sections. As for the Xianxia-Jianhe intersection, the dispersion degree gradually reaches the maximum at the 20-meter marker and then

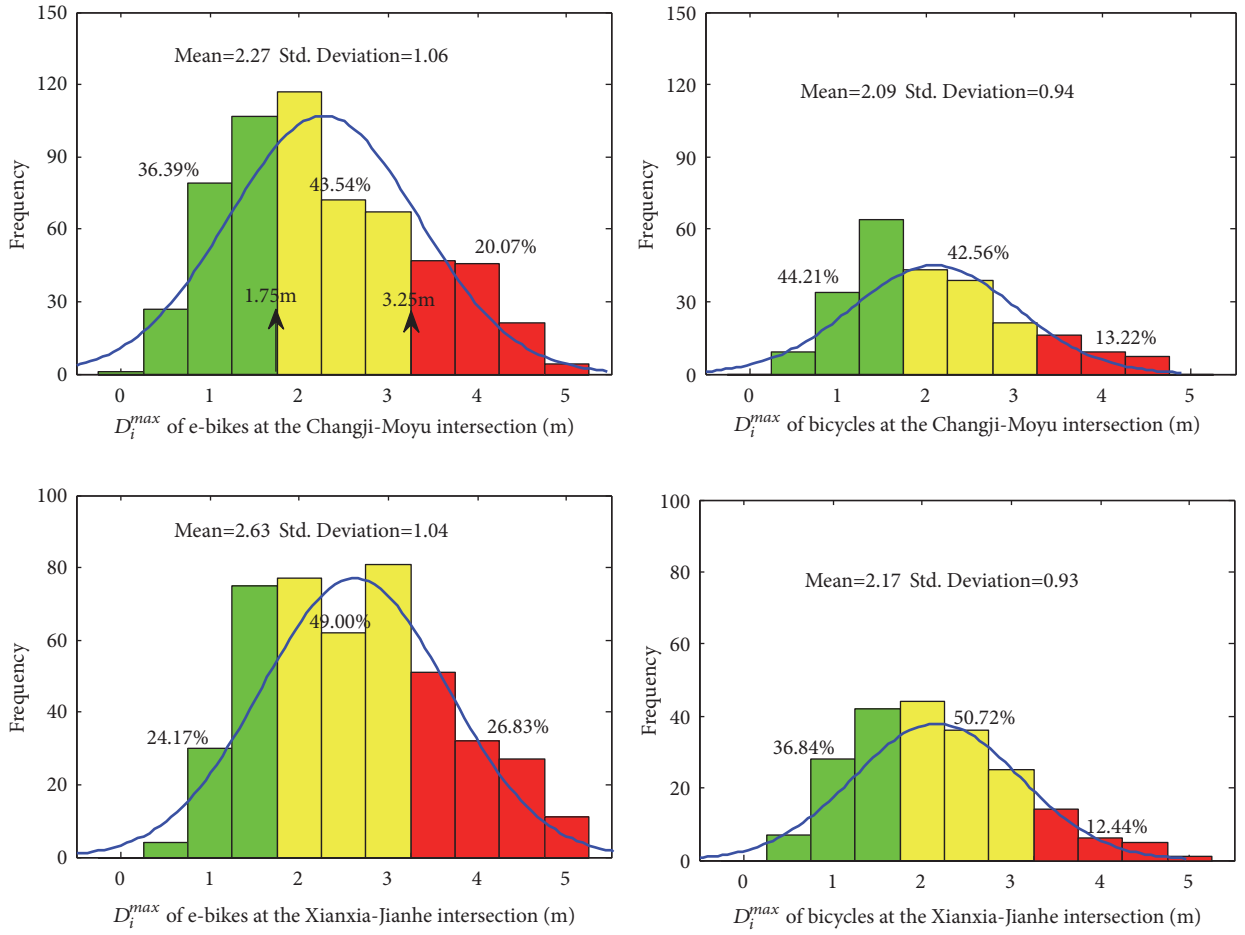

Figure 8: Histograms of D_i^{max} for e-bikes and bicycles at both intersections.

Table 1: Parameters of the binary logistic model at two intersections.

Location	Parameter	Value	S.E.	Sig.	Percentage correct of the model	Critical boundary δ_r^{max} ($P(D_i^{max}) = 0.5$)
Changji-Moyu intersection	B_1	-6.122	1.194	0.000	96.4%	3.067
	B_2	18.793	3.658	0.000		
Xianxia-Jianhe intersection	B_1	3.623	0.661	0.000	94.1%	3.191
	B_2	-11.50	2.004	0.000		

gradually decreases back to 1.0. Such differences might be due to the difference in the geometric design as well as the composition of the nonmotorized and motorized vehicles at two intersections.

The maximum sectional dispersion degree λ_x determines the maximum lateral dispersion position. Seven factors that may influence the maximum sectional dispersion degree were further selected and they are (1) the number of go-straight, nonmotorized vehicles, (2) the number of go-straight, nonmotorized vehicles queued at the stop line when the traffic light turns green, (3) the number of pedestrians, (4) the ratio of e-bikes, (5) the average speed of the e-bikes, (6) the average speed of bicycles, and (7) the go-straight motorized vehicle's time occupancy in the adjacent lane. A correlation analysis between the maximum sectional dispersion degree is conducted and the results are summarized in Table 2.

The result shows that the maximum sectional dispersion degree has a positive correlation with the number of go-straight, nonmotorized vehicles queued at the stop line and a negative correlation with the go-straight motorized vehicle's time occupancy. These conclusions help set up the model for depicting the dispersion behavior of go-straight, nonmotorized vehicles.

Based on the preliminary analysis of the dispersing nonmotorized vehicles, two important characteristics are discovered and should be captured in the model. (1) The

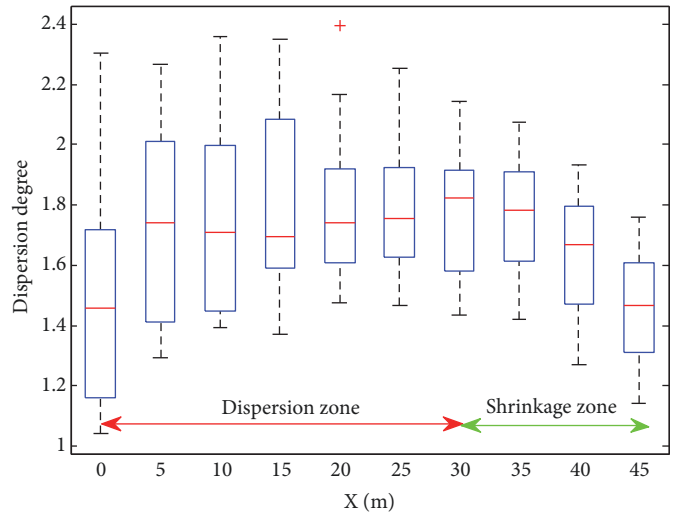

Figure 9: Boxplot of sectional dispersion degree at Changji-Moyu intersection.

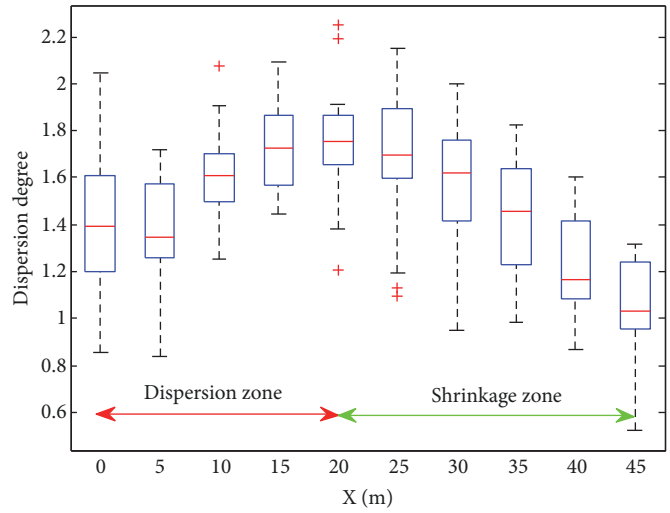

Figure 10: Boxplot of sectional dispersion degree at Xianxia-Jianhe intersection.

dispersion intensity, such as the dispersion ratio and the maximum lateral offset distance, differs between e-bikes and bicycles. The e-bikes have a relatively stronger intensity of dispersion. (2) The nonmotorized vehicle groups behave in a "dispersion and shrinkage" way during the crossing process. The average dispersion boundary is serpentine.

4. Methodology

4.1. Basic Idea. Conventional models for nonmotorized vehicles summarized in literature review, including the virtual lane model, the SFM, and the CA model, cannot depict the two essential characteristics mentioned in the previous section.

In this paper, we were inspired by the dispersion of charged particles in an electric field and decided to adopt the charged particles behavior model to depict the dispersion phenomenon of go-straight, nonmotorized vehicles. The macroscopic nonmotorized vehicles and the microscopic charged particles share three inherent commonalities with regard to the forces directly applied on them. First, a driving force is applied on the charged particle as the destination panel has an opposite sign of charge and attracts the particle. The nonmotorized vehicles also experience such a driving force, as the ultimate objective of the nonmotorized vehicle is to exit the intersection as soon as possible. Therefore, the exit lane attracts the nonmotorized vehicles. Second, charged particles within the electric field experience repulsive forces from other particles, and such repulsive forces increase as the speed of particle increases. It is the same for nonmotorized vehicles in that nonmotorized vehicles experience repulsive forces from other nonmotorized vehicles, and such repulsive forces increase if the nonmotorized vehicle's speed increases, since nonmotorized vehicles are more likely to maintain a longer clearance distance with others under high-speed

Table 2: Results of the correlation analysis in between of the maximum sectional dispersion degree and 7 dynamic factors.

	Dynamic factors	Parameters	Value
Maximum sectional dispersion degree	Number of go-straight non-motorized vehicles	Pearson Correlation	-0.038
		P-value	0.790
	Number of go-straight non-motorized vehicles queued at stop line	Pearson Correlation	*0.324***
		P-value	0.014
	The number of pedestrians	Pearson Correlation	-0.012
		P-value	0.231
	Ratio of e-bikes	Pearson Correlation	-0.096
		P-value	0.500
	Average speed of non-motorized vehicles	Pearson Correlation	-0.195
		P-value	0.040
	Average speed of motorized vehicles in adjacent lane	Pearson Correlation	0.094
		P-value	0.562
	Go-straight motorized vehicle's time occupancy in adjacent lane	Pearson Correlation	*-0.772***
		P-value	0.000

*Correlation is significant at the 0.05 level (2-tailed).
**Correlation is significant at the 0.01 level (2-tailed).

Table 3: Similarities between the dispersion of charged particles in electric fields and nonmotorized vehicles' dispersion at intersections.

Dispersion characteristics	Dispersion of charged particle in electric field (microscopic field)	Dispersion of non-motorized vehicles at intersections (macroscopic space)
Dispersion and shrinkage process	Charged particles dispersing to electric boundary will shrink back to the field [41]	Go-straight non-motorized vehicles will disperse and shrink during the crossing process (Figures 9 and 10)
Dispersion intensity	Particle with higher charge quantity disperses with higher intensity since a higher repulsive force is applied to them [41]	High-speed e-bike has a stronger intension to disperse (Figure 8)
Distance among participants	The distances between charged particles increases if their speeds increase [40]	The distance between non-motorized vehicles will increase if the non-motorized vehicles' speeds increase [46]

scenarios. Third, particles are repelled from the upper and lower boundaries as they hold the same sign of electric charge. As for nonmotorized vehicles, they are also repelled from the inner motorized vehicle lane as vehicles wish to avoid motorized vehicles and return to the nonmotorized vehicle lane laterally near the exit of the intersection.

When a charged particle beam (or group) starts to move along the longitudinal direction in an unrestricted field, it disperses in the field laterally. The lateral dispersion distance has a positive correlation with the speed v_i of the electron i, the charge quantity q_i of electron i, the electric field intensity E, and the longitudinal moving distance l_a [40]. If a boundary exists in the field, the laterally dispersing electron will shrink when it approaches the boundary [41]. There are three key similarities between the charged particles' dispersion in a restricted electric field and nonmotorized vehicles' dispersion at intersections. These similar characteristics are documented in Table 3.

The charged particle beam (or group) departs from the starting panel and moves towards the ending panel. Such a moving field has upper and lower boundaries. The starting panel and boundaries have the same sign of electric charge with the charged particle beam while the ending panel has the opposite sign of electric charge. The particles in the electric field are affected by three forces: the driving force F_i^d, the boundary force F_i^b, and the repulsive force F_{ij}^{α}.

The driving force F_i^d is calculated as

$$F_i^d = \frac{4\pi k q_i \left(Q_o + Q_d\right)}{S} \tag{5}$$

where k is the electrostatic constant, q_i denotes the quantity of electric charge on particle i, Q_0 and Q_d denote the electric quantity of the starting panel and the ending panel, and S is the overlapping area of the starting and ending panels. The driving force of the particle i has positive relationship

with the quantity of electric charge q_i, the electric quantity in the starting panel Q_o, and the ending panel Q_d. It has the negative relationship with the overlapping area of starting panel and the ending panel. When the overlapping area is smaller, the electron on the starting panel and the ending panel will be more concentrated. The driving force in the electric field will be stronger as a result.

The boundary force F_i^b is calculated as

$$F_i^b = k\frac{q_i \cdot Q_b}{d_b^2} \tag{6}$$

where Q_b denotes the electric quantity of the upper/lower boundary and d_b denotes the distance from particle i to the upper or lower boundary. The boundary force has the positive relationship with the quantity of electric charge q_i, the electric quantity of upper/lower boundary. It has the negative relationship with the square of distance to upper boundary or lower boundary. The direction of the boundary force is perpendicular to the boundary.

The repulsive force F_{ij}^{α} [42] on particle i from another particle j is calculated as

$$F_{ij}^{\alpha} = k\frac{q_i \cdot q_j}{d^2} \tag{7}$$

where d denotes the distance between particles i and j. The repulsive force has a negative relationship with the square of the distance between the two particles. The direction of repulsive force is from j to i.

This model can only describe the dispersion process of particle groups with a fixed boundary but cannot depict the shrinkage process. At the same time, there is no limit to the speed and acceleration of the charged particles so that the speed of the charged particles can increase forever. Moreover, the repulsive force of the particles comes from all particles in the electric field while the nonmotorized vehicles may only experience repulsion from front nonmotorized vehicles. Therefore, this model is further upgraded to consider the following items: (1) dynamic dispersion boundary: go-straight, nonmotorized vehicles may have varying dispersion boundaries in each cycle, (2) shrink force: when nonmotorized vehicle groups move to a certain position, the dispersing nonmotorized vehicles will shrink into the regulation zone and exit the intersection, and (3) repulsive force and maximum speed: generally speaking, go-straight nonmotorized vehicles only receive a repulsive force from nonmotorized vehicles in front, and the speed cannot exceed a maximum threshold.

4.2. Particle Dispersion Model for Go-Straight Nonmotorized Vehicles. In this paper, a PDM is proposed to depict the go-straight, nonmotorized vehicles' dispersion phenomenon. The model is developed based upon the particle moving model in an electric field with an enhancement implemented to address the issues mentioned in the previous section. The forces applied upon the go-straight, nonmotorized vehicles in the dispersion area are as shown in Figure 11.

In the PDM, the nonmotorized vehicle i will move from the stop line to the exit line under four forces: the driving force $\overrightarrow{F_i^{dP}}$, the boundary force $\overrightarrow{F_i^{bP}}$, the repulsive force $\overrightarrow{F_i^{\alpha P}}$, and the shrink force $\overrightarrow{F_i^{sP}}$. The coordinate of the nonmotorized vehicle i in the system is (x_i, y_i). The resultant force $\overrightarrow{F_i^P}$ on nonmotorized vehicle i is defined in

$$\overrightarrow{F_i^P} = \overrightarrow{F_i^{dP}} + \overrightarrow{F_i^{bP}} + \overrightarrow{F_i^{\alpha P}} + \overrightarrow{F_i^{sP}} \tag{8}$$

The four kinds of forces are given as follows.

(1) Driving Force $\overrightarrow{F_i^{dP}}$. The driving force of nonmotorized vehicle i is $\overrightarrow{F_i^{dP}}$, and the unit is N. The force is given by

$$\overrightarrow{F_i^{dP}} = \frac{4\pi k_P q_i^P \left(Q_o^P + Q_d^P\right)}{S_P} \cdot \overrightarrow{n_d^P} \tag{9}$$

where k_P is a parameter that needs to be calibrated, Q_o^P denotes the width of the nonmotorized vehicle lane at the approach of the intersection, and Q_d^P denotes the width of the nonmotorized vehicle lane at the exit of the intersection. S_P is defined as $w*w$. $\overrightarrow{n_d^P}$ is the unit vector of the force direction (1,0). q_i^P is the momentum of the nonmotorized vehicle i and is calculated by

$$q_i^P = \beta_P \cdot v_i \tag{10}$$

where β_P is a parameter that needs to be calibrated and v_i is the current speed of nonmotorized vehicle i. q_i^P is so defined because the moving intensity is found to have positive linear relationship with v_i as per the observations in field data.

(2) Boundary Force $\overrightarrow{F_i^{bP}}$. The boundary force is given by

$$\overrightarrow{F_i^{bP}} = \begin{cases} k_P \dfrac{q_i^P \cdot Q_b^P}{\left(d_{EB}^P\right)^2} \cdot \overrightarrow{n_{EB}^P}, & y_i > \dfrac{w}{2} \\ 0, & -\dfrac{w}{2} \le y_i \le \dfrac{w}{2} \\ k_P \dfrac{q_i^P \cdot Q_b^P}{\left(d_{FB}^P\right)^2} \cdot \overrightarrow{n_{FB}^P}, & y_i > -\dfrac{w}{2} \end{cases} \tag{11}$$

where Q_b^P is the length of the nonmotorized vehicle lane at the intersection and $\overrightarrow{n_{EB}^P}$ and $\overrightarrow{n_{FB}^P}$ are unit vectors of the force direction with values of (0, -1) and (0, 1), respectively. d_{BE}^P is the distance between nonmotorized vehicle i and the upper boundary (elastic boundary shown in Figure 11) and d_{BF}^P is the distance between nonmotorized vehicle i and the lower boundary (fixed boundary shown in Figure 11). The fixed boundary is lateral offset w (see (1)) from the nonmotorized vehicle lane, so the distance between the fixed boundary and the center line of the nonmotorized vehicle lane is $1.5w$. d_{BE}^P and d_{BF}^P are defined in

$$d_{BE}^P = y_E - y_i \tag{12}$$

$$d_{BF}^P = y_i - 1.5w \tag{13}$$

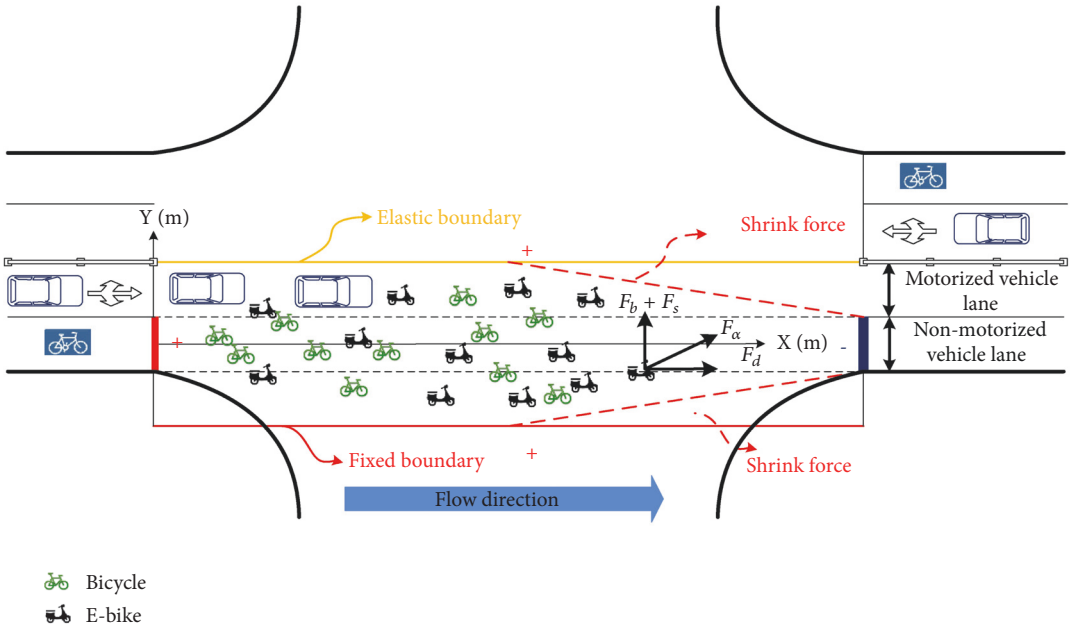

Figure 11: Forces in the dispersion model.

where y_E is the elastic boundary location and is presented in

$$y_E = f(n_c, O_c) \tag{14}$$

where n_c is the number of queuing nonmotorized vehicles at the stop line in cycle c. O_c is the time occupancy of go-straight, nonmotorized vehicles in cycle c. This equation needs to be fitted based on the field data.

(3) Repulsive Force $\overrightarrow{F_i^{\alpha P}}$. When the nonmotorized vehicle i is moving in the area, the repulsive force from the front nonmotorized vehicle j is defined in

$$\overrightarrow{F_{ij}^{\alpha P}} = \begin{cases} k_P \dfrac{q_i^P \cdot q_j^P}{d_{ij}^2} \cdot \overrightarrow{n_{ij}}, & x_i < x_j \\ 0, & x_j \le x_i \end{cases} \tag{15}$$

where d_{ij}^2 is the distance between the nonmotorized vehicle i and the nonmotorized vehicle j. $\overrightarrow{n_{ij}}$ is the unit vector of the force direction (pointing from j to i). The resultant repulsive force from all nonmotorized vehicles in front is given by

$$\overrightarrow{F_i^{\alpha P}} = \sum_{j=1}^{N_f} \overrightarrow{F_{ij}^{\alpha P}} \tag{16}$$

where N_f is the number of nonmotorized vehicles in front of nonmotorized vehicle i.

(4) Shrink Force $\overrightarrow{F_i^{sP}}$. As observed in the field data, the nonmotorized vehicle will gradually shrink back to the regulation zone once it reaches the 20-30m marker. Therefore, it is assumed that the nonmotorized vehicle begins to shrink when it reaches the middle of the intersection for the sake of simplicity. For the shrink force of the nonmotorized vehicle, the closer the nonmotorized vehicle is to the exit of the intersection, the greater the force is. The shrink force $\overrightarrow{F_i^{sP}}$ is calculated as

$$\overrightarrow{F_i^{sP}} = \begin{cases} 0, & x_i \le \dfrac{L}{2} \\ \dfrac{k_P \cdot q_i^P \cdot Q_b^P \cdot (x_i - L/2)}{(L/2) \cdot x_i} \cdot \overrightarrow{n_{EB}^P}, & x_i > \dfrac{L}{2},\ y_i > \dfrac{w}{2} \\ \dfrac{k_P \cdot q_i^P \cdot Q_b^P \cdot (x_i - L/2)}{(L/2) \cdot x_i} \cdot \overrightarrow{n_{FB}^P}, & x_i > \dfrac{L}{2},\ y_i < -\dfrac{w}{2} \end{cases} \tag{17}$$

where L is the length of the intersection. Lastly, the acceleration $\overrightarrow{\alpha_i}$ of nonmotorized vehicle i is calculated as

$$\overrightarrow{\alpha_i^P} = \frac{\overrightarrow{F_i^P}}{m_i} \tag{18}$$

where m_i is the mass of nonmotorized vehicle i. $\overrightarrow{\alpha_i^P}$ is the acceleration of nonmotorized vehicle i. In addition, the maximum speed of the nonmotorized vehicle is set according to the field data.

5. Simulation and Results Analysis

5.1. Parameter Calibration of the PDM. Despite the differences in terms of the geometric designs between the two

Table 4: Observed and calibrated parameters of the PDM.

Type of Parameter	Parameter	Value of parameters	Description
Observed Parameters	w	3.5	Width of non-motorized vehicle lane (m)
	L	47	Length of non-motorized vehicle lane (m)
	v_i^0	(6.48,1.56)	Mean and std. deviation of e-bikes' desired speed (m/s)
		(4.05,1.64)	Mean and std. deviation of bicycles' desired speed (m/s)
	a_i^0	(0.75,0.42)	Mean and std. deviation of e-bikes' max acceleration (m/s^2)
		(0.52,0.27)	Mean and std. deviation of bicycles' max acceleration (m/s^2)
	m_i	115	Mass of e-bike (kg)
		75	Mass of bicycle (kg)
Calibrated Parameters	k_P	2.201	Force coefficient
	β_P	1.998	Momentum coefficient

intersections of interest, the objective of the model is to be generalizable and thus would be adopted as a universal model for any general intersections. Therefore, the data collected at the Changji-Moyu intersection was used for model calibration and the data collected at the Xianxia-Jianhe intersection was used for model validation. Based on the previous description of the PDM, there are three kinds of parameters that should be calibrated, and they are the elastic boundary parameters, the observed parameters, and the calibrated parameters.

n_c and O_c in (11) should be fitted for the elastic boundary location. There exist multiple options for the form of the equation, so the curve fitting toolbox in MATLAB was utilized and the most suitable equation was obtained as follows:

$$y_E = 0.1829 + 0.0721n_c + 3.3657e^{-(19.93O_c)^2} \quad (19)$$

within which the goodness of fit R^2 is 0.933.

The observed parameters at the Changji-Moyu intersection are presented in Table 4. Based on (19) and the observed parameters, a genetic algorithm (GA) was applied to calibrate the rest of the parameters in the PDM. In the calibration, GA was adopted to minimize the relative error between the simulated aggregate travel times and extracted aggregate travel times of all the nonmotorized vehicles at the Changji-Moyu intersection. The time step of the simulation is 0.12s, which is the same with the extracted data. The objective function for the relative travel time error $g(t)$ is given by

$$g(t) = \frac{1}{N}\sum_{1}^{N} t_i^P - \frac{1}{N}\sum_{1}^{N} t_i \quad (20)$$

where t_i^P denotes the travel time of nonmotorized vehicle i in the PDM and t_i denotes the travel time of nonmotorized vehicle i in the field data. The initial range of k_P and β_P is from 0 to 20. Once the average change in the fitness value reaches lower than 0.01%, the iterative optimization terminates. The observed and calibrated parameters of the PDM are summarized in Table 4.

The calibrated parameters were then applied to the Xianxia-Jianhe intersection.

5.2. Parameter Calibration of the SFM. The SFM is widely adopted for depicting nonmotorized vehicles' driving behavior and the forces emulated within the SFM are similar to that in the PDM [4, 22, 23, 43]. Therefore, the simulated results obtained by the PDM were compared to those obtained by the SFM in this study. The standard social force model includes the driving force $\overrightarrow{F_i^{dS}}$, the boundary force $\overrightarrow{F_i^{bS}}$, and the repulsive force $\overrightarrow{F_i^{\alpha S}}$. The resultant force is $\overrightarrow{F_i^S}$.They are summarized in the following equations.

$$\overrightarrow{F_i^S} = \overrightarrow{F_i^{dS}} + \overrightarrow{F_i^{bS}} + \overrightarrow{F_i^{\alpha S}} \quad (21)$$

$$\overrightarrow{F_i^{dS}} = \frac{1}{\tau}\left(\overrightarrow{v_i^0} - \overrightarrow{v_i}\right) \quad (22)$$

$$\overrightarrow{F_i^{bS}} = \mathrm{A}_B e^{-d_B^S/\mathrm{B}_B} \cdot \overrightarrow{n_B^S} \quad (23)$$

$$\overrightarrow{F_i^{\alpha S}} = \sum_{j=1}^{N_f} \overrightarrow{F_{\alpha ij}^S} = \sum_{j=1}^{N_f} \mathrm{A}_v \omega e^{-d_{ij}/\mathrm{B}_v} \times \overrightarrow{n_{ij}} \quad (24)$$

where $\overrightarrow{v_i^0}$ denotes the desired speed of nonmotorized vehicle I and $\overrightarrow{v_i}$ denotes the current speed of nonmotorized vehicle i. τ is the relaxation time. $1/\tau$ represents the value of tendency to approach desired speed $\overrightarrow{v_i^0}$. $\overrightarrow{n_B^S}$ is the unit vector pointing from bound to influenced nonmotorized vehicle, $\overrightarrow{n_{ij}}$ is the unit vector pointing from influencing j to influenced nonmotorized vehicle i as (13), d_B^S is the distance from nonmotorized vehicle i to the upper or lower boundary, d_{ij} is the distance between nonmotorized vehicle i, and a nonmotorized vehicle j in front. A_v, B_v, A_B, and B_B are calibrated parameters. The upper and lower boundaries in the SFM are the same as with the PDM. The calibration process

Table 5: Observed and calibrated parameters of SFM.

Type of Parameter	Parameter	Value of parameter	Description
Observed Parameter	v_i^0	(6.48,1.56)	Mean and std. deviation of e-bikes' desired speed (m/s)
		(4.05,1.64)	Mean and std. deviation of bicycles' desired speed (m/s)
Calibrated Parameter	τ	13.03	Buffer time of driving force
	A_v	0.610	Repulsive force of other non-motorized vehicle users
	B_v	0.841	
	A_B^l	0.401	Lower boundary force
	B_B^l	19.554	
	A_B^u	0.352	upper boundary force
	B_B^u	9.207	

is similar to what was shown in the previous calibration procedure for the PDM. Meanwhile, the elastic boundary and the shrink force in the SFM are the same as the PDM as shown in (14) and (17).

There are one observed parameter and seven calibrated parameters in the SFM. A GA [44, 45] is adopted to minimize the relative error between the simulated aggregate travel times and observed aggregate travel times of all nonmotorized vehicles at the Changji-Moyu intersection. The observed and calibrated parameters obtained by the GA are given in Table 5.

5.3. Results Analysis. In this section, the travel time is compared since it is the principal output of traffic flow simulation. Then, the analysis of the three important dispersion characteristics is presented: the dispersion ratio, the dispersion intensity, and the sectional dispersion degree. Lastly, the spatial-temporal distribution of all nonmotorized vehicles is presented.

5.3.1. Travel Time. In this paper, travel time is adopted to calibrate the parameters in the PDM and SFM at the Changji-Moyu intersection and the calibrated model is then applied to the other intersection directly. The cumulative probability curves of travel time for all nonmotorized vehicles at both intersections are shown in Figures 12 and 13.

From Figure 13, one can easily tell that the PDM is superior to the SFM in describing the travel times of nonmotorized vehicles at the intersection for validation. A paired t-test was conducted, and it shows that the distributions of travel time are obtained by the PDM and that from the field data belong to the same distribution (P value is 0.09 at the Changji-Moyu intersection and 0.17 at the Xianxia-Jianhe intersection). On the other hand, the SFM largely underestimates the travel time of nonmotorized vehicles for the Xianxia-Jianhe intersection.

5.3.2. Dispersion Ratio and Dispersion Intensity. In order to evaluate the model performance for different types of dispersing nonmotorized vehicle (e-bike and bicycle), the total number of dispersing/high dispersion intensity e-bikes and bicycles is compared. The results are shown in Figures 14 and 15.

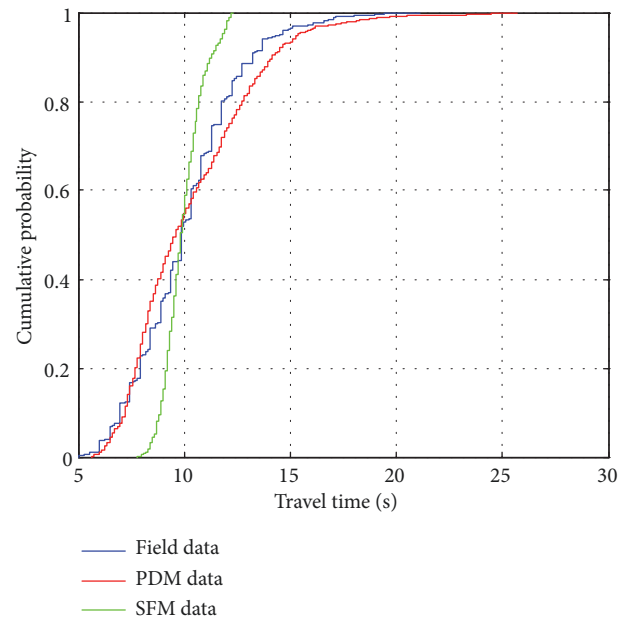

Figure 12: Cumulative probability curve of the travel time at the Changji-Moyu intersection.

From those two figures one can tell that the PDM outperforms the SFM at both intersections. Since the number of dispersing nonmotorized vehicles is not the objective for calibration, the SFM largely underestimates the number of dispersing and high dispersion nonmotorized vehicles, even for the calibration intersection. It also reveals that the SFM is not capable of depicting the dispersion phenomenon.

5.3.3. Sectional Dispersion Degree. Next, the "dispersion-shrinkage" process of nonmotorized vehicle groups simulated in the PDM and SFM are compared. The simulated sectional dispersion degrees at two intersections are compared

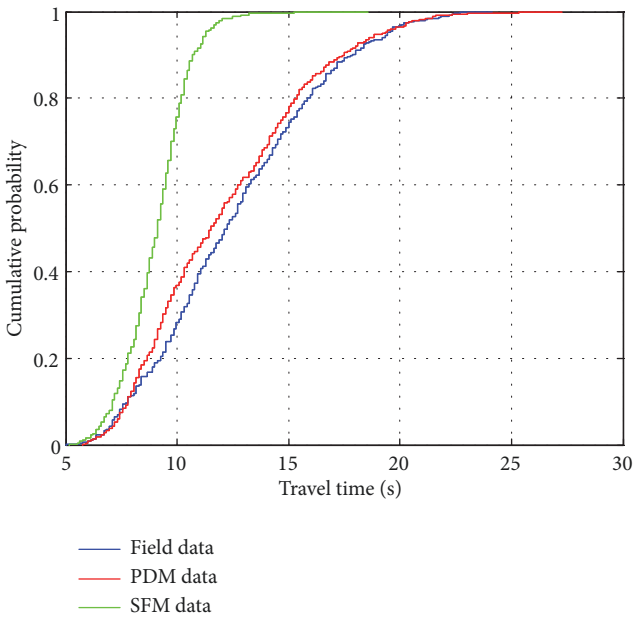

Figure 13: Cumulative probability curve of the travel time at the Xianxia-Jianhe intersection.

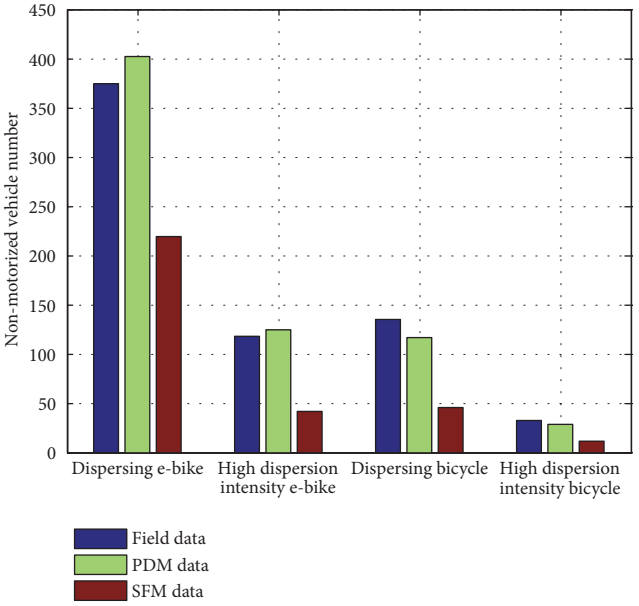

Figure 14: Number of dispersing nonmotorized vehicles at the Changji-Moyu intersection.

with field data. There are 19 values (19 cycles) in each section at the Changji-Moyu intersection and 24 values (24 cycles) in each section at the Xianxia-Jianhe intersection. The median values in each section are shown in Figures 16 and 17.

First, the dispersion zone is roughly from 0 m to 25 m at the Changji-Moyu intersection as observed in the field data. The PDM successfully replicates such outputs (there is only a 5 m offset as the dispersion zone obtained by the PDM is 0 m to 30 m) while the SFM fails as dispersion after 5 m is never observed in the simulated results of the

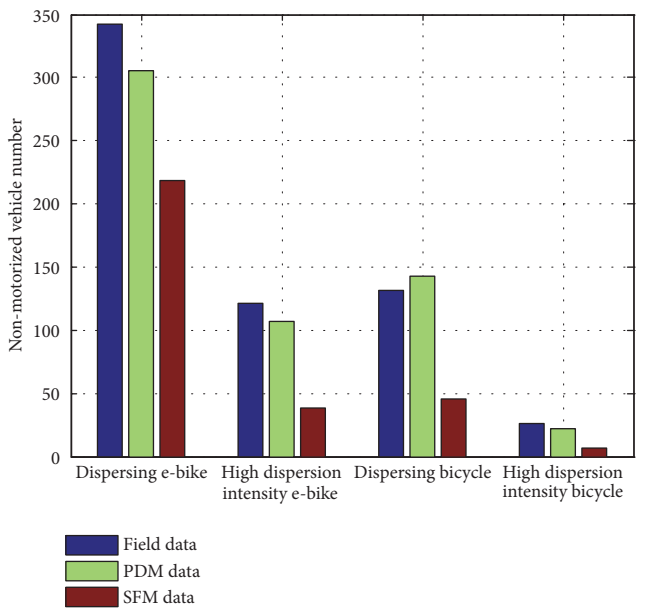

Figure 15: Number of dispersing nonmotorized vehicles at the Xianxia-Jianhe intersection.

SFM. Similar patterns are observed at the Xianxia-Jianhe intersection, that the PDM's prediction of the dispersion zone is exactly the same as the field data (0m to 20 m). In the SFM, the nonmotorized vehicles shrink from the origin to the destination. It cannot describe the "dispersion-shrinkage" phenomenon at all, which also explains why there are much fewer dispersing nonmotorized vehicles observed in the SFM as shown in the previous section.

Second, the difference of the median dispersion degree between the simulated and observed data is calculated. The results show that the average error in each section is 4.33% at the Changji-Moyu intersection and 4.96% at the Xianxia-Jianhe intersection in the PDM simulation, which is much lower than the 39.02% and 28.78% achieved with SFM simulation, respectively.

5.3.4. Distribution of Nonmotorized Vehicles. To analyze the location of all nonmotorized vehicles at both intersections, the heat maps of the trajectories of nonmotorized vehicles are presented in Figures 18 and 19.

One can tell that the PDM is capable of accurately replicating the dispersion and shrink procedures, while the SFM fails. Since the SFM is not capable of depicting the dispersion phenomenon, nonmotorized vehicles shrink to a small region in the SFM and there is no dispersion zone in the middle of the intersection as shown in the field data. In the meantime, the destination in the SFM is fixed and thus the trajectories concentrate to a small region at the end, which is not the case in field data.

It is not feasible to compare the trajectory of each individual nonmotorized vehicle at the microscopic level as stochastic factors exist. RMSE is used to evaluate the

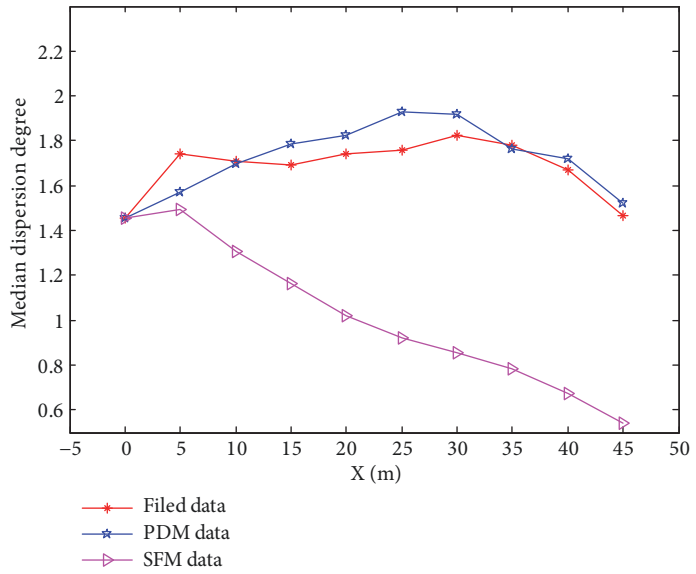

Figure 16: Median dispersion degree in each section at the Changji-Moyu intersection.

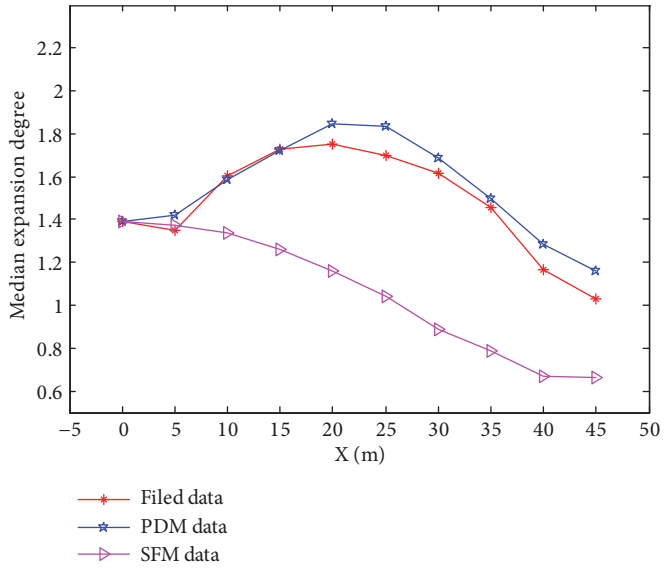

Figure 17: Median dispersion degree in each section at the Xianxia-Jianhe intersection.

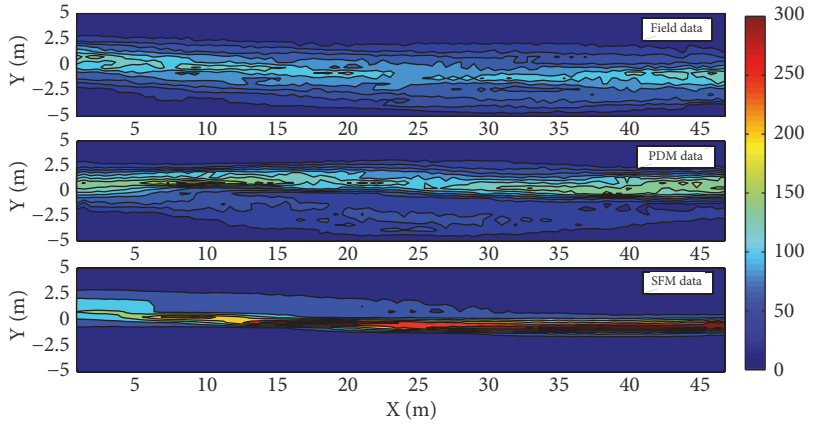

Figure 18: Distribution of nonmotorized vehicles at the Changji-Moyu intersection.

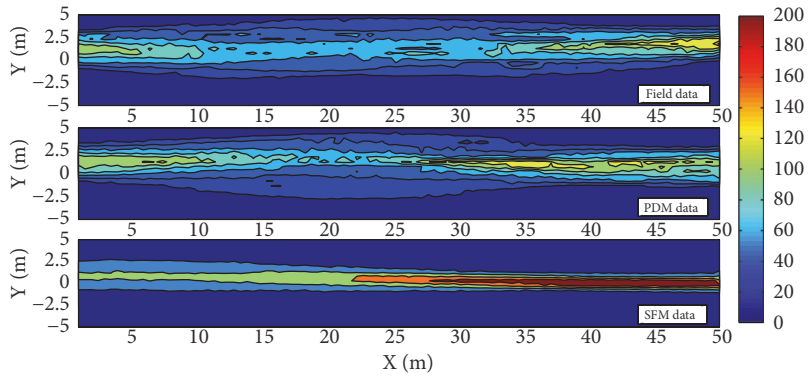

Figure 19: Distribution of nonmotorized vehicles at the Xianxia-Jianhe intersection.

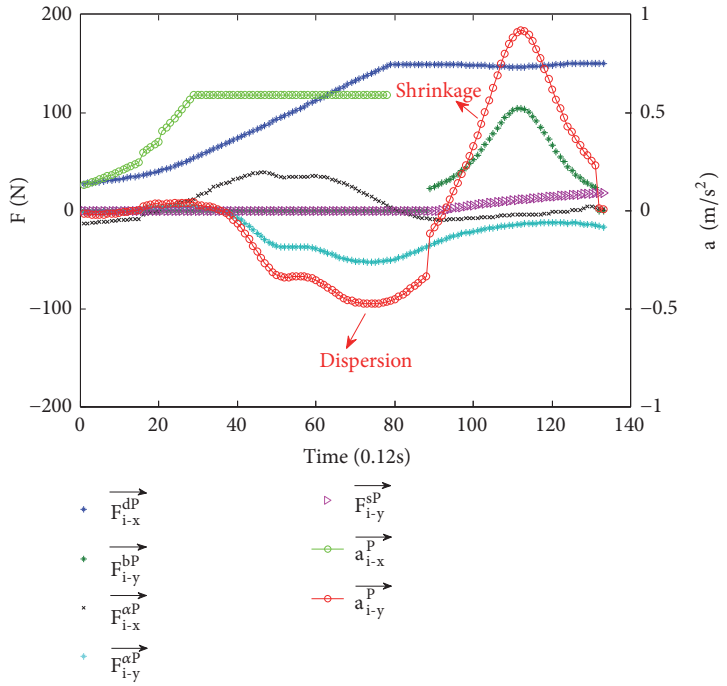

Figure 20: Force and acceleration in the PDM.

distribution of nonmotorized vehicles at an aggregate level herein and is given as

$$\mathrm{RMSE}_{\lambda} = \sqrt{\frac{1}{Z}\sum_{i=1,j=1}^{Z}\left(m_{ij} - m_{ij}^{\lambda}\right)^2}, \quad \lambda = PDM \text{ or } SFM \tag{25}$$

where m_{ij} is the frequency that the nonmotorized vehicles appear in the grid ij in field data, and $m_{ij} \neq 0$. Z is the total number of grids with m_{ij} not equal to 0. m_{ij}^{λ} is the frequency that the nonmotorized vehicles appear in the grid ij in simulated trajectory data. λ is set to either the PDM or SFM. The lower the RMSE is, the better-fit the model is.

The RMSE score of the PDM simulation is 44.72 at the Changji-Moyu intersection, and the score of the SFM is 70.09. The RMSE score of the PDM simulation is 20.44 at the Changji-Moyu intersection, and the SFM simulation achieves 53.35, which is much worse than the PDM.

5.4. Insights and Discussion. Furthermore, in order to reveal the causes of nonmotorized vehicles' dispersion phenomenon in the PDM and to explain why the SFM is not able to depict such phenomenon, the lateral and longitudinal forces and acceleration of a typical dispersing nonmotorized vehicle in a typical cycle are plotted, and the results are shown in Figures 20 and 21. The force and acceleration for a dispersing nonmotorized vehicle in the PDM are shown in Figure 20.

It can be seen from Figure 20 that this dispersing nonmotorized vehicle experiences a lateral mutual repulsion force $\overrightarrow{F_{i-y}^{\alpha P}}$ (x and y mean the longitudinal and latitudinal direction of the force, respectively) at the beginning of the trip and that the force pushes the nonmotorized vehicle to disperse out of

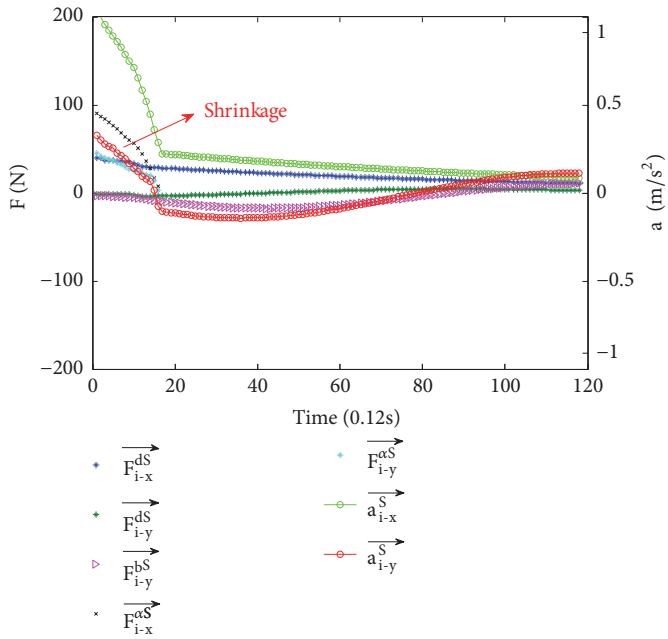

Figure 21: Force and acceleration in the SFM.

the regulation zone. Once the nonmotorized vehicle reaches close to the boundary, the lateral boundary force $\overrightarrow{F^{bP}_{i-y}}$ and shrink force $\overrightarrow{F^{sP}_{i-y}}$ pull the dispersing nonmotorized vehicle back into regulation zone. The dispersion zone and shrinkage zone are distinct during the go-straight process as shown in Figure 20. Meanwhile the longitudinal acceleration $\overrightarrow{a^{P}_{i-x}}$ and latitudinal acceleration $\overrightarrow{a^{P}_{i-y}}$ are within the normal range based on the field data shown in Table 4.

Figure 21 shows the forces and acceleration of the same nonmotorized vehicle in the SFM simulation. In the SFM, the result of the force is the acceleration and the unit for force is N, meaning that the force in the SFM is equal to the acceleration multiplied by the mass of the nonmotorized vehicle. The destination in the SFM is a single fixed point during the whole process of crossing, rather than a dynamic adjustable destination in the PDM. Furthermore, once the nonmotorized vehicle departs heading to the destination, the lateral boundary force $\overrightarrow{F^{dS}_{i-y}}$ remains at a low value because the nonmotorized vehicle is too close to the lane center and too far away from the boundary. Therefore, the nonmotorized vehicle stays at the lane center at the beginning of the trip and remains at the lane center thereafter. Thus, the nonmotorized vehicle does not disperse in the SFM.

6. Conclusion and Future Work

This paper presents a novel particle dispersion model (PDM) for simulating the dispersion phenomenon of nonmotorized vehicles. The PDM had been calibrated and validated using 1,490 high precision trajectory data sets at two typical mixed flow intersections. The main conclusions of the paper are summarized as follows:

(i) The nonmotorized vehicles have obvious dispersion phenomenon at mixed flow intersections. More than 68% of go-straight, nonmotorized vehicles disperse out of the regular driving zone at the two studied intersections. Compared to bicycles, e-bikes have a stronger dispersion intensity. The average of the maximum lateral offset distance is 2.27m and 2.63m for e-bikes at the two intersections and 2.09m and 2.17m for bicycles at the two intersections, respectively.

(ii) The PDM can describe the dispersion phenomenon with clear physical meanings and less parameters. The PDM is derived from the microphysics realm and the mechanism (with four types of forces) in the model shows that it has a great advantage in depicting the successive dispersion and shrinkage phenomenon of nonmotorized vehicles over a conventional SFM.

(iii) The PDM can simulate nonmotorized vehicle flow and has higher accuracy when describing dispersion characteristics. Four kinds of indices have been validated and compared with the field collected trajectories: the travel time, the dispersion ratio, the sectional dispersion degree, and the distribution of all nonmotorized vehicles. Results show that the PDM not only can describe the nonmotorized flow accurately, but also achieves better performance compared to the widely used SFM model.

In the future, it is planned to explore modified SFMs that may be able to better depict the dispersion phenomenon as benchmark. Besides, to extend the PDM to depict the behavior of nonmotorized vehicles on intersections with different configurations and basic road sections and to further

integrate it with microscopic traffic simulation packages to establish an integrated simulation model for nonmotorized traffic flow under various scenarios is worthy of further exploration.

Data Availability

The nonmotorized vehicle trajectory data used to support the findings of this study are available from the corresponding author upon request.

Conflicts of Interest

The authors declare that there are no conflicts of interest regarding the publication of this paper.

Acknowledgments

This research was sponsored by the Natural Science Foundation of China (U1764261), the "Shuguang Program" supported by Shanghai Education Development Foundation and Shanghai Municipal Education Commission (18SG21), and the Science and Technology Commission Shanghai Municipality (16DZ1203602).

References

[1] L. Bai, P. Liu, Y. Chen, X. Zhang, and W. Wang, "Comparative analysis of the safety effects of electric bikes at signalized intersections," *Transportation Research Part D: Transport and Environment*, vol. 20, pp. 48–54, 2013.

[2] B. Langford, J. Chen, and C. Cherry, "Risky riding: naturalistic methods comparing safety behavior from conventional bicycle riders and electric bike riders," *Accident Analysis & Prevention*, vol. 82, pp. 220–226, 2015.

[3] R. Rash-ha Wahi, N. Haworth, A. K. Debnath, and M. King, "Influence of type of traffic control on injury severity in bicycle–motor vehicle crashes at intersections," *Transportation Research Record*, Article ID 0361198118773576, 2018.

[4] D. Allen, J. Hummer, N. Rouphail, and J. Milazzo, "Effect of bicycles on capacity of signalized intersections," *Transportation Research Record: Journal of the Transportation Research Board*, vol. 1646, Article ID 16461998, pp. 87–95, 1998.

[5] S. J. Mok, E. C. Kim, and H. B. Heo, "A study on efficient management of bicycle traffic flow at four-legged intersections," *Journal of the Korean Society of Road Engineers*, vol. 15, no. 3, pp. 177–189, 2013.

[6] Y. Guo, Q. Yu, Y. Zhang, and J. Rong, "Effect of bicycles on the saturation flow rate of turning vehicles at signalized intersections," *Journal of Transportation Engineering*, vol. 138, no. 1, pp. 21–30, 2011.

[7] D. Huang, D. L. Qian, and C. L. Zhao, "Study on behavior of right-turning motor crossing go-straight non-motorized vehicles at grade intersection," *Journal of Beijing Jiaotong University*, vol. 3, no. 005, 2006.

[8] Y. Wang and N. L. Nihan, "Estimating the risk of collisions between bicycles and motor vehicles at signalized intersections," *Accident Analysis & Prevention*, vol. 36, no. 3, pp. 313–321, 2004.

[9] Z. Ma, J. Xie, X. Qi, Y. Xu, and J. Sun, "Two-dimensional simulation of turning behavior in potential conflict area of mixed-flow intersections," *Computer-Aided Civil and Infrastructure Engineering*, vol. 32, no. 5, pp. 412–428, 2017.

[10] Z. Ma, J. Sun, and Y. Wang, "A two-dimensional simulation model for modelling turning vehicles at mixed-flow intersections," *Transportation Research Part C: Emerging Technologies*, vol. 75, pp. 103–119, 2017.

[11] J. Chen, W. Wang, Z. Li, H. Jiang, X. Chen, and S. Zhu, "Dispersion effect in left-turning bicycle traffic and its influence on capacity of left-turning vehicles at Signalized intersections," *Transportation Research Record*, vol. 2468, no. 1, pp. 38–46, 2014.

[12] J. Broker and M. M. Hottman, *Bicycle Accidents, Crashes, and Collisions: Biomechanical, Engineering, and Legal Aspects*, TRB, 2016.

[13] G. Ren, H. Jiang, J. Chen, Z. Huang, and L. Lu, "Heterogeneous cellular automata model for straight-through bicycle traffic at signalized intersection," *Physica A: Statistical Mechanics and its Applications*, vol. 451, pp. 70–83, 2016.

[14] J. Dill, C. M. Monsere, and N. McNeil, "Evaluation of bike boxes at signalized intersections," *Accident Analysis & Prevention*, vol. 44, no. 1, pp. 126–134, 2012.

[15] D. H. Wang, T. J. Feng, and C. Y. Liang, "Research on bicycle conversion factors," *Transportation Research Part A: Policy and Practice*, vol. 42, no. 8, pp. 1129–1139, 2008.

[16] H. Jiang, Y. Ma, L. Jiang, G. Chen, and D. Wang, "Evaluation of the dispersion effect in go-straight movement bicycles at signalized intersection via cellular automata simulation," *Physica A: Statistical Mechanics and its Applications*, vol. 498, pp. 138–147, 2018.

[17] S. I. Khan and P. Maini, "Modeling heterogeneous traffic flow," *Transportation Research Record: Journal of the Transportation Research Board*, vol. 1678, pp. 234–241, 1999.

[18] H. Ling and J. Wu, "A study on cyclist behavior at signalized intersections," *IEEE Transactions on Intelligent Transportation Systems*, vol. 5, no. 4, pp. 293–299, 2004.

[19] H. Jiang, G. Ren, L. Zheng, J. Chen, and Z. Huang, "Properties analyses for the heterogeneous nonmotorized vehicle traffic based on cellular automaton model," *International Journal of Modern Physics B*, vol. 28, no. 16, Article ID 1450099, 2014.

[20] H. Twaddle, T. Schendzielorz, and O. Fakler, "Bicycles in urban areas: Review of existing methods for modeling behavior," *Transportation Research Record*, vol. 2434, no. 1, pp. 140–146, 2014.

[21] J. Barceló, *Fundamentals of Traffic Simulation*, vol. 145, Springer International Publishing, New York, NY, USA, 2010.

[22] M. Li, F. Shi, and D. Chen, "Analyze bicycle-car mixed flow by social force model for collision risk evaluation," in *Proceedings of the 3rd International Conference on Road Safety and Simulation*, pp. 1–22, 2011.

[23] L. Huang, J. Wu, F. You, Z. Lv, and H. Song, "Cyclist social force model at unsignalized intersections with heterogeneous traffic," *IEEE Transactions on Industrial Informatics*, vol. 13, no. 2, pp. 782–792, 2017.

[24] X. Liang, M. A. O. Baohua, and X. U. Qi, "Psychological-physical force model for bicycle dynamics," *Journal of Transportation Systems Engineering and Information Technology*, vol. 12, no. 2, pp. 91–97, 2012.

[25] R. Schönauer, M. Stubenschrott, W. Huang, C. Rudloff, and M. Fellendorf, "Modeling concepts for mixed traffic: steps toward a microscopic simulation tool for shared space zones,"

Transportation Research Record, vol. 2316, no. 1, pp. 114–121, 2012.

[26] K. Nagel and M. Schreckenberg, "A cellular automation model for freeway traffic," *Journal de Physique I*, vol. 2, no. 12, pp. 2221–2229, 1992.

[27] D. Yao, Y. Zhang, L. Li, Y. Su, S. Cheng, and W. Xu, "Behavior modeling and simulation for conflicts in vehicles-bicycles mixed flow," *IEEE Intelligent Transportation Systems Magazine*, vol. 1, no. 2, pp. 25–30, 2009.

[28] Y. J. Luo, B. Jia, J. Liu, W. H. K. Lam, X. G. Li, and Z. Y. Gao, "Modeling the interactions between car and bicycle in heterogeneous traffic," *Journal of Advanced Transportation*, vol. 49, no. 1, pp. 29–47, 2015.

[29] K. Tang, S. Dong, F. Wang, Y. Ni, and J. Sun, "Behavior of riders of electric bicycles at onset of green and yellow at signalized intersections in China," *Transportation Research Record: Journal of the Transportation Research Board*, vol. 2317, pp. 85–96, 2012.

[30] J. Sun, K. Zuo, S. Jiang, and Z. Zheng, "Modeling and predicting stochastic merging behaviors at freeway on-ramp bottlenecks," *Journal of Advanced Transportation*, vol. 2018, Article ID 9308580, 15 pages, 2018.

[31] GB 50220-95, "Code for transport planning on urban road," 1995.

[32] D. Yang, X. Zhou, D. Wu, and S. Liu, "Study on the invasion behavior of E-bikes with motor vehicle traffic at a signalized intersection," *Transportation Research Record*, vol. 2672, no. 31, pp. 33–40, 2018.

[33] Y. Guo, Z. Li, Y. Wu, and C. Xu, "Exploring unobserved heterogeneity in bicyclists' red-light running behaviors at different crossing facilities," *Accident Analysis & Prevention*, vol. 115, pp. 118–127, 2018.

[34] X. Zang, Y. Tang, X. Zhang, and X. Hu, "Former analysis of side interference for mixed traffic," *Technology & Economy in Areas of Communications*, vol. 2, no. 3, pp. 54-55, 2000.

[35] H. Guan, M. Wang, and H. Chi, "Study on road traffic delay caused by bicycle for mixed traffic stream," *Journal of Beijing Polytechnic University*, vol. 3, no. 013, 2005.

[36] J. I. A. Shunping, P. E. N. G. Hongqin, G. U. O. Jinyi, and C. H. E. N. Haibo, "Quantitative analysis of impact of bicycles on vehicles in urban mixed traffic," *Journal of Transportation Systems Engineering and Information Technology*, vol. 8, no. 2, pp. 58–63, 2008.

[37] D. Carter L, W. Hunter, C. Zegeer V, J. R. Stewart, and H. F. Huang, "Pedestrian and bicyclist intersection safety indices," 2006.

[38] H. Botma, "Method to determine level of service for bicycle paths and pedestrian-bicycle paths," *Transportation Research Record*, no. 1502, pp. 38–44, 1995.

[39] R. D. Bock and R. Mislevy, *BILOG 3: Item analysis & test scoring with binary logistic models*, Scientific Software International, Incorporated, 1990.

[40] R. P. Feynman, R. B. Leighton, and M. Sands, *The Feynman Lectures on Physics: Mainly Electromagnetism and Matter*, vol. 2, 1977.

[41] D. Dubbers, L. Raffelt, B. Märkisch, F. Friedl, and H. Abele, "The point spread function of electrons in a magnetic field, and the decay of the free neutron," *Nuclear Instruments and Methods in Physics Research Section A: Accelerators, Spectrometers, Detectors and Associated Equipment*, vol. 763, pp. 112–119, 2014.

[42] R. J. Zauhar and R. S. Morgan, "A new method for computing the macromolecular electric potential," *Journal of Molecular Biology*, vol. 186, no. 4, pp. 815–820, 1985.

[43] F. Pascucci, N. Rinke, C. Schiermeyer, B. Friedrich, and V. Berkhahn, "Modeling of shared space with multi-modal traffic using a multi-layer social force approach," *Transportation Research Procedia*, vol. 10, pp. 316–326, 2015.

[44] W. Zeng, P. Chen, G. Yu, and Y. Wang, "Specification and calibration of a microscopic model for pedestrian dynamic simulation at signalized intersections: A hybrid approach," *Transportation Research Part C: Emerging Technologies*, vol. 80, pp. 37–70, 2017.

[45] B. Anvari, M. G. H. Bell, A. Sivakumar, and W. Y. Ochieng, "Modelling shared space users via rule-based social force model," *Transportation Research Part C: Emerging Technologies*, vol. 51, pp. 83–103, 2015.

[46] S. Zhang, G. Ren, and R. Yang, "Simulation model of speed-density characteristics for mixed bicycle flow—comparison between cellular automata model and gas dynamics model," *Physica A: Statistical Mechanics and its Applications*, vol. 392, no. 20, pp. 5110–5118, 2013.

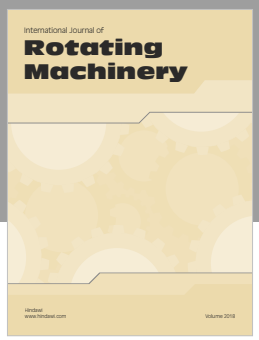

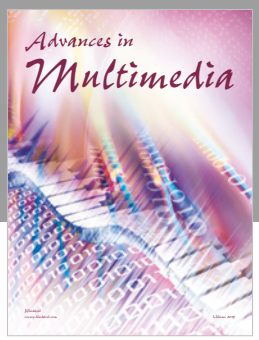

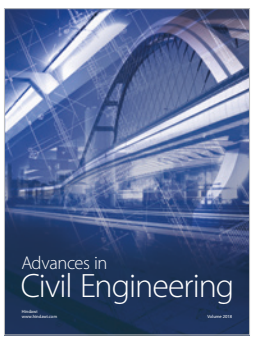

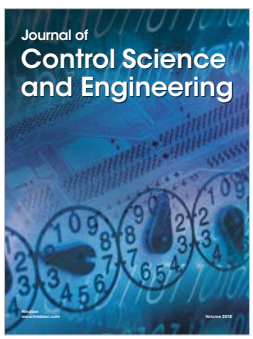

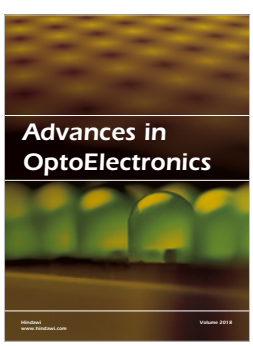

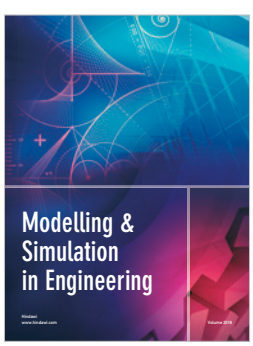

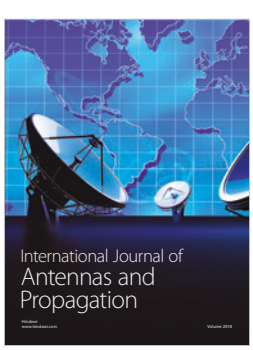

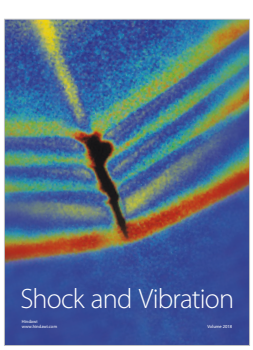

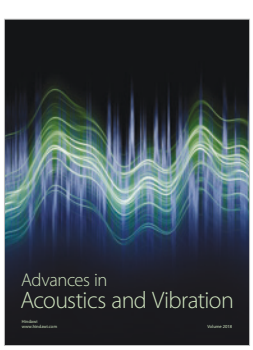

Hindawi

Submit your manuscripts at
www.hindawi.com